A New Approach for Ferrocenyl-Cyclopentenone and Ferrocenyl-Cyclopentenedione Compound Synthesis

Jie Li, Jian-Ping Ma, Fengling Liu, Xiang-Wen Wu, Yu-Bin Dong,* and Ru-Qi Huang

College of Chemistry, Chemical Engineering and Materials Science, Key Laboratory of Molecular and Nano Probe, Engineering Research Center of Pesticide and Medicine Intermediate Clean Production, Ministry of Education, Shandong Normal University, Jinan, 250014, People's Republic of China

Received March 16, 2008

A simple and convenient route for the synthesis of the ferrocenyl-cyclopentenone compounds (**3** and **7**) and ferrocenyl-cyclopentenedione compounds (**4** and **8**) has been developed. Compounds **3** and **7** were obtained by a selective oxidating reaction of the ferrocenyl-cyclopenta[*d*]pyridazine species of **2** and **6** in CH_2Cl_2 in air, respectively. Compounds **4** and **8** were generated by a hydrolysis reaction of **3** and **7** in a H_2O/EtOH mixed solvent system in the presence of $SnCl_2$, respectively. The substituted ferrocenyl group plays a central role in the formation of the ferrocenyl-cyclopentenone (**3** and **7**) and ferrocenyl-cyclopentenedione (**4** and **8**) derivatives, which is demonstrated well by the current experimental data as well as the theoretical calculations. All the new ferrocene-containing complexes have been characterized by elemental analysis, IR spectra, and ^{1}H NMR spectroscopy, as well as for **3**, **4**, **5**, **7**, **8**, and **9** by X-ray diffraction analysis. In addition, the luminescent properties of **1**−**4** were investigated preliminarily in CH_2Cl_2 at room temperature.

Introduction

The widespread importance of cyclopentyl compounds has led to numerous methods for their synthesis.[1] Cyclopentenone and cyclopentenedione derivatives are particularly useful compounds that have vast importance in biology, medicine, and chemistry due to their versatility of functionality.[2] For instance, cyclopentenone prostaglandins exhibiting a characteristic biological activity and soft acid-type electrophilic cyclopentendione moiety are good candidates for antitumor drug design.[3] The classical methods for their synthesis involve the intramolecular aldol reaction of a selected 1,5-diketone and the metal-mediated approach, which was developed by Pauson and Khand.[2a,4] On the other hand, conjugated ferrocene-containing organic molecules have emerged as an important class of materials with numerous applications; for example, the Fe(II)/Fe(III) redox couple has been widely used in redox-active sensing applications because it is readily available and exhibits "well-behaved" electrochemistry and photochromism.[5] We wondered if the electro-active moiety, ferrocene, could be combined with the cyclopentenone or cyclopentenedione species to generate new types of functional molecules, such as complex biologically active molecules, which are potentially used as the electro-probe to explore the biological activity and drug working mechanism. In this contribution, we report a new and convenient approach for the synthesis of ferrocene-containing cyclopentenone and cyclopentenedione derivatives.

Results and Discussion

Synthesis and Characterization of 1−4. We have been interested in the synthesis of new fulvene molecules by aroylation of the substituted cyclopentadienyl anion and the organometallic coordination polymers based on them.[6] Motivated by our interest, we have initiated a synthetic program for the preparation of new organometallic fulvene molecules and their reaction chemistry, in which FcCOCl and ferrocenyl-substituted aroyl chloride are used instead of aroyl chloride to perform the reactions. The aroylation of cyclohexyl-substituted cyclopentadienyl anion by FcCOCl resulted in **1** as red-orange crystalline solids in moderate yield.[6h] The same as its phenyl or heterocycle terminal-substituted fulvene analogues,[6a,b] **1** readily reacted with hydrazine in EtOH at reflux to generate **2** as yellow-orange crystalline solids in quantitative yield. In the ^{1}H NMR spectra, a single peak related to the imine group was observed at 13.11 ppm, which is about 5 ppm shifted to higher field compared to the proton resonance (18.20 ppm) of the hydroxy hydrogen on its precursor **1**. The IR spectrum of **2** showed a sharp −NH absorption band at 3379 cm^{-1}. The strong

* Corresponding author. E-mail: yubindong@sdnu.edu.cn.

(1) (a) Trost, B. M.; Toste, F. D. *J. Am. Chem. Soc.* **2000**, *122*, 714. (b) Buchwald, S. L. *J. Am. Chem. Soc.* **1999**, *121*, 7026.

(2) (a) Gibson, S. E.; Mainolfi, N. *Angew. Chem., Int. Ed.* **2005**, *44*, 3022. (b) Gibson, S. E.; Stevenazzi, A. *Angew. Chem., Int. Ed.* **2003**, *42*, 1800. (c) Hori, H.; Nagasawa, H.; Ishibashi, M.; Uto, Y.; Hirata, A.; Saijo, K.; Ohkura, K.; Kirk, K. L.; Uehara, Y. *Bioorg. Med. Chem.* **2002**, *10*, 3257.

(3) (a) Straus, D. S.; Glass, C. K. *Med. Res. Rev.* **2001**, *21*, 185. (b) Moos, P. J.; Edes, K.; Cassidy, P.; Massuda, E.; Fitzpatrick, F. A. *J. Biol. Chem.* **2003**, *278*, 745.

(4) Khand, I. U.; Knox, G. R.; Pauson, P. L.; Watts, W. E. *J. Chem. Soc. D* **1971**, 36.

(5) (a) Wang, K.; Muńoz, S.; Zhang, L.; Castro, R.; Kaifer, A. E.; Gokel, G. W. *J. Am. Chem. Soc.* **1996**, *118*, 6707. (b) Hillard, E.; Vessières, A.; Thouin, L.; Jaouen, G.; Amatore, C. *Angew. Chem., Int. Ed.* **2006**, *45*, 285. (c) Sakamato, R.; Murata, M.; Nishihara, H. *Angew. Chem., Int. Ed.* **2006**, *45*, 4793.

(6) (a) Dong, Y.-B.; Geng, Y.; Ma, J.-P.; Huang, R.-Q. *Organometallics* **2006**, *25*, 447. (b) Dong, Y.-B.; Geng, Y.; Ma, J.-P.; Huang, R.-Q. *Inorg. Chem.* **2005**, *44*, 1693. (c) Wang, P.; Dong, Y.-B.; Ma, J.-P.; Huang, R.-Q.; Smith, M. D. *Crystal Growth Des.* **2005**, *5*, 701. (d) Dong, Y.-B.; Wang, P.; Huang, R.-Q.; Smith, M. D. *Inorg. Chem.* **2004**, *43*, 4727. (e) Dong, Y.-B.; Jin, G.-X.; Zhao, X.; Huang, R.-Q.; Smith, M. D.; Stitzer, K. E.; zur Loye, H.-C. *Organometallics* **2004**, *23*, 1604. (f) Dong, Y.-B.; Ma, J.-P.; Jin, G.-X.; Huang, R.-Q.; Smith, M. D. *Dalton Trans* **2003**, *22*, 4324. (g) Dong, Y.-B.; Jin, G.-X.; Smith, M. D.; Tang, B.; zur Loye, H.-C. *Inorg. Chem.* **2002**, *41*, 4909. (h) Jiao, L.-J.; Liu, G.-H.; Ma, Y.-D.; Dong, Y.-B. *Chin. J. Org. Chem.* **1995**, *15*, 259.

10.1021/om800246s CCC: $40.75
Publication on Web 10/10/2008

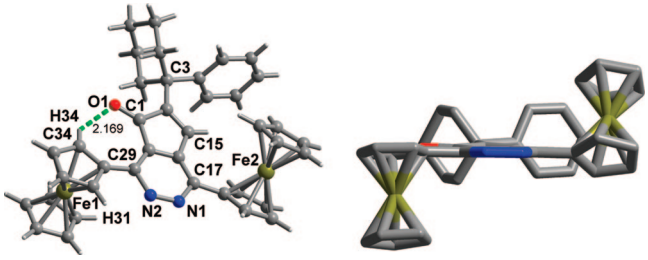

Figure 1. Molecular structure of **3**.

absorption bands at 1594 and 1369 cm^{-1} are consistent with the >C═N and fulvene adsorptions, respectively, which are comparable to the corresponding bands in known compounds.[6] Thus, the H-bonded seven-membered ring of **1** was replaced by a six-membered hydropyridazino moiety in **2**.

We were delighted to find that, upon exposure to air for 12 h at room temperature (monitored by TLC), solution of **2** in CH_2Cl_2 reacted cleanly to form the novel ferrocenyl-cyclopentenone **3** as deep-green crystalline solids in good yield. In contrast to the ^1H NMR spectra of **1** and **2**, no proton resonance was found in the downfield (>10 ppm) region with respect to the loss of the active hydrogen on the N atom in **3**. In addition, the IR spectrum of **3** showed a 1713 cm^{-1} absorption derived from the typical conjugated carbonyl, which is reflected in the oxidation restricted to the C−H bond.

The cyclopentadiene moiety in **2** was oxidized to cyclopentadienone species **3**, which was further confirmed by its X-ray single-crystal structure. The single-crystal X-ray diffraction analysis revealed that **2** was oxidated at the central fulvene ring instead of ferrocene. As shown in Figure 1, the C(1)−H(1) bond in **2** was oxidized to C(1)═O(1). The two ferrocenyl groups attached to the pyridazino ring in **3** were located above and below the cyclopentadienone- hydropyridazino plane in the solid state. One of the two substituted ferrocenyl groups (Fe(1)) was fixed by one set of intramolecular hydrogen bonds ($d_{O(1)\cdots H(34)}$ = 2.2 Å, $d_{O(1)\cdots C(34)}$ = 2.9 Å and ∠O(1)−H(34)−C(34) = 135°), which might be the reason for the ferrocenyl proton signals splitting up into four groups, which is compatible with the assigned structure.

Molecular oxygen is a highly desirable oxidant from chemical, environmental, and economic standpoints. However, the effective utilization of O_2 in selective C−H oxidation reactions still remains a great challenge due to a very limited understanding of how transition metal complexes activate either the C−H bond or O_2. Significant recent progress in the use of metal complex catalysts for selective aerobic oxidations has emphasized the importance of developing a thorough comprehension of reactions between metal complexes, O_2, and C−H substrates.[7] Herein, it is no doubt that such novel selective oxidation on the C−H bond was promoted by the ferrocenyl substituents, which was demonstrated well by our experiments. For example, when the solutions of the analogues of **2** in CH_2Cl_2, such as phenyl or heterocycle terminal-substituted fulvene molecules,[6] were allowed to stand in air for several days, no oxidated products were detected. In addition, parallel reactions carried out under ambient light and in the dark showed comparable rates for the formation of **3**, which strongly suggests that the oxidation of **2** to **3** did not proceed via a light-induced radical mechanism.

(7) (a) Shilov, A. E.; Shteinman, A. A. *Acc. Chem. Res.* **1999**, *32*, 763. (b) Merkx, M.; Kopp, D. A.; Sazinsky, M. H.; Blazyk, J. L.; Müller, J.; Lippard, S. J. *Angew. Chem., Int. Ed.* **2001**, *40*, 2782. (c) Stahl, S. S. *Angew. Chem., Int. Ed.* **2004**, *43*, 3400.

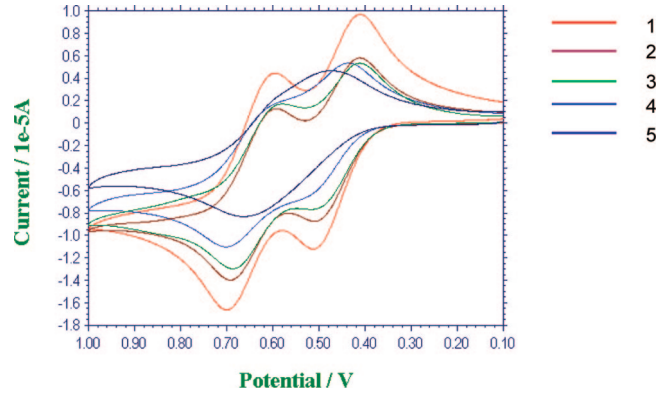

Figure 2. Consecutive cyclic voltammogram from **2** (trace 1) to **3** (trace 5) in CH_2Cl_2.

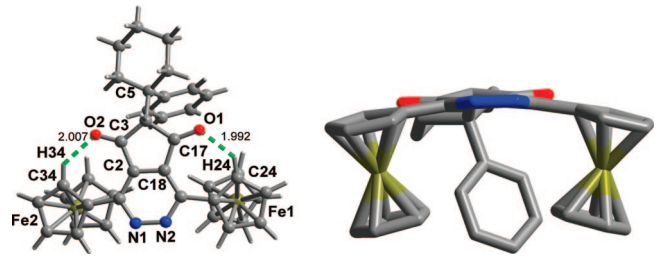

Figure 3. Molecular structure of **4**.

The whole oxidiation process of **2** in air was monitored by CV (Figure 2). As expected, the cyclic voltammetric response in methylene chloride solution in air indicated that the diferrocenyl complex **2** underwent two oxidation steps ($E_{1/2}$ = 487 and 675 mV). As time went on, the double redox waves of **2** overlapped gradually and the redox waves of **3** formed finally. No long-lived intermediates are involved during the oxidation process. Compared to ferrocene ($E_{1/2}$ = 0.41−0.42 V), the voltammograms for **2** and **3** reveal an anodic shift due to the adjacent electron-withdrawing imine units.

It is interesting that **3** is not prone to further oxidation in air at room temperature. The Fc-cyclopentenedione **4**, however, could be obtained as purple crystalline solids by the hydrolysis of **3** in the presence of $SnCl_2$ at room temperature in good yield (75%). When **3** was treated with several drops of water in EtOH in the presence of $SnCl_2$ under N_2 atmosphere, compound **4** was obtained in the same yield; however, the reaction carried out in anhydrous EtOH in the presence of $SnCl_2$ in dry air did not lead to the formation of **4**. These parallel reactions confirmed that the formation of **4** from **3** went through a hydrolytic process instead of an oxidating process. X-ray single-crystal analysis revealed that the hydrolysis happened on the other sp^2 carbon atom, C(17), of the central cyclopentenone ring (Figure 3). Different from **3**, two terminal ferrocenyl substituents of **4** are fixed by two sets of intramolecular hydrogen bonds ($d_{O(2)\cdots H(34)}$ = 2.0 Å, $d_{O(2)\cdots C(34)}$ = 2.7 Å and ∠O(2)−H(34)−C(34) = 134°; $d_{O(1)\cdots H(24)}$ = 2.0 Å, $d_{O(1)\cdots C(24)}$ = 2.7 Å and ∠O(1)−H(24)−C(24) = 137°), respectively, which gave rise to the ferrocenyl proton signals splitting up into five groups in its ^1H NMR spectrum. The side view of **4** indicated that both ferrocenyl groups are symmetrically located on the same side of the cyclopentenedione-hydropyridazino plane in the solid state (Figure 3).

The UV/vis spectra of **1**−**4** are characterized by a strong absorption band at 303 nm (ϵ = 1.48 × 10^4 M^{-1} cm^{-1}) (**1**), 306 nm (ϵ = 1.60 × 10^4 M^{-1} cm^{-1}) (**2**), 303 nm (ϵ = 1.55 × 10^4 M^{-1} cm^{-1}) (**3**), and 295 nm (ϵ = 9.49 × 10^3 M^{-1} cm^{-1}) (**4**), respectively, which are assigned to a high-energy $\pi-\pi^*$

Scheme 1. Synthesis of Compounds 1 (red), 2 (yellow), 3 (green), and 4 (purple) in CH_2Cl_2

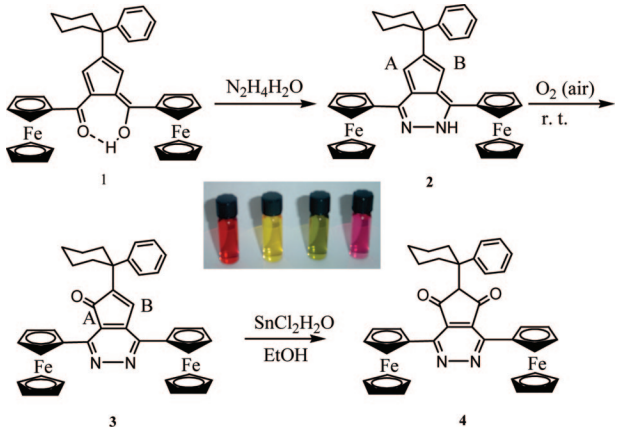

Scheme 2. Synthesis of Compounds 5 (red-orange), 6 (light yellow), 7 (brown), and 8 (light brown) in CH_2Cl_2

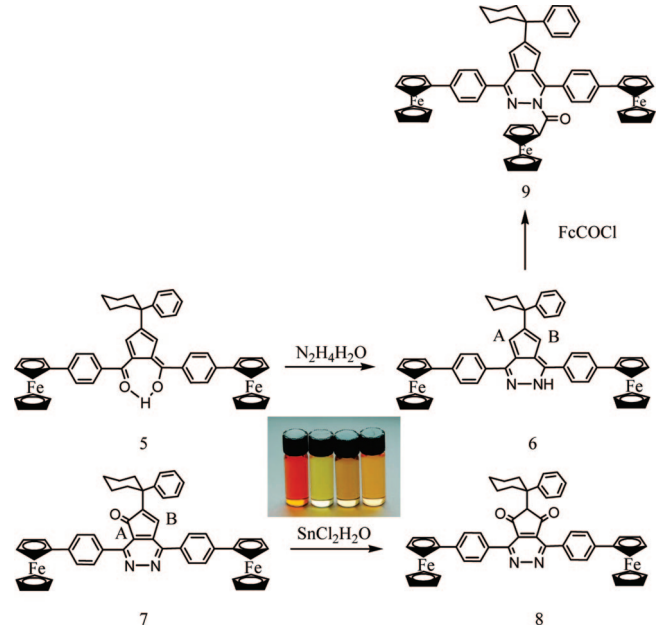

electronic transition, and moderate absorption bands at 436 nm ($\epsilon = 1.14 \times 10^4$ M^{-1} cm^{-1}) (**1**), 442 nm ($\epsilon = 2.73 \times 10^3$ M^{-1} cm^{-1}) (**2**), 367 nm ($\epsilon = 5.44 \times 10^3$ M^{-1} cm^{-1}) (**3**), and 339 nm ($\epsilon = 1.24 \times 10^4$ M^{-1} cm^{-1}) (**4**), which are attributed to a n$-\pi^*$ electronic transition. The lower energy weaker bands at 518 nm ($\epsilon = 7.72 \times 10^3$ M^{-1} cm^{-1}) (**1**), 521 nm ($\epsilon = 1.55 \times 10^3$ M^{-1} cm^{-1}) (**3**), and 527 nm ($\epsilon = 3.40 \times 10^3$ M^{-1} cm^{-1}) (**4**) correspond to the metal-to-ligand charge transfer process (d$-\pi^*$).[8] Such spectral features confer a series of color changes from **1** to **4** (Scheme 1), which enables us to easily monitor the reactions by the naked eye. In addition, all four complexes are strongly luminescent in CH_2Cl_2 at room temperature ($\lambda_{ex}/\lambda_{em}$ (nm): 364/410 (**1**), 367/410 (**2**), 363/411 (**3**), and 367/411 (**4**)); they exhibit similar fluorescence spectra due to their similar conjugated systems (Figure 4).

Synthesis and Characterization of 5−9. In order to further confirm this interesting chemical phenomenon related to ferrocene-substituted fulvene compounds, we designed and synthesized compound **5**, which is generated from ferrocenyl benzoyl chloride. As shown in Scheme 2, compound **5** was obtained as red-orange crystalline solids by the aroylation of cyclohexyl-substituted cyclopentadienyl anion by 4-FcC_6H_4-COCl in a relatively low yield (25%). The X-ray single-crystal structural analysis revealed that **5** and **1** are isostructural but with two longer side arms. The distance between the two Fe(II) centers in **5** is 17.554 Å, and the two terminal ferrocenyl groups are perpendicular to each other in the solid state (Figure 5). As for **1**, compound **5** could condense with hydrazine in dry ethanol to generate a cyclopenta[*d*]pyridazine derivative as the yellow-orange crystalline solid **6** in 93% yield. In comparison to **2**, compound **6** in methylene chloride could also be oxidized by O_2 to its cyclopentenone species **7** upon exposure to air, but it took a longer time (72 h, monitored by TLC), which is probably due to the effective electron delocalization caused by the larger conjugated system in **6**.

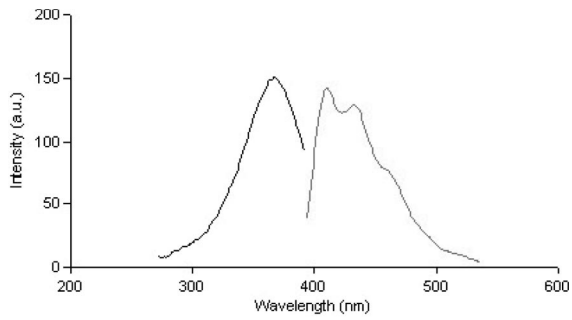

Figure 4. Photoinduced excitation (black line) and emission (gray line) spectra of **1** in CH_2Cl_2.

The single-crystal structure of **7** shows that one of the C−H bonds on the central cyclopentadiene ring was activated and oxidized to a >C═O group. It is different from **5** in that the two terminal ferrocenyl groups are located on both sides of the central plane and point in the opposite directions (Figure 6). Again, in EtOH solution, **7** underwent clean hydrolysis reaction to produce **8** at room temperature, which has been confirmed by ^{1}H NMR, elemental analysis, and X-ray diffraction. The transformation rates of **7** to **8** and **3** to **4** are comparative. As shown by the diagrams in Figure 7, the phenyl ring attached to the quaternary carbon atom (C(21)) bends markedly to the pyridazine plane and interacts with it through a weak $\pi-\pi$ stacking interaction. The two ferrocenyl groups in **8** are parallel and point in the same direction.

As shown in Scheme 2, reaction of compound **6** with excess FcCOCl in dry CH_2Cl_2 afforded the triferrocenyl compound **9**. The absorption band corresponding to the −NH group disappeared, whereas the new strong absorption band at 1710 cm^{-1} is in good agreement with the carbonyl attached to the nitrogen atom. The ^{1}H NMR spectrum of **9** displayed a multiplet at 4.02−4.81 ppm assigned to 27 Cp protons, which are attributed to the three Fc groups. The molecular structure of **9** was unambiguously confirmed by crystal X-ray diffraction analysis. The ORTEP view of **9** is presented in Figure 8, and selected bond lengths and angles are given in Table 2. Compared to **6**, one more Fc group was attached to the central cyclopenta[*d*]-pyridazine moiety bridged by a carbonyl.

Similar to compounds **1**−**4**, UV−vis spectra of **5**−**9** in CH_2Cl_2 show strong absorption bands, which are assigned to a high-energy $\pi-\pi^*$ electronic transition and a n$-\pi^*$ electronic transition, respectively (Table 3). Compared to **1**−**4**, compounds **5**−**9**, however, do not show significant photoluminescence.

As shown in Table 4, the cyclic voltammogram data of **6**−**8** show one quasi-reversible redox wave, while **9** shows two quasi-reversible redox waves, which corresponds to a [Fe^{III}/Fe^{II}] process. Compared to **2** and **3**, the half-wave potentials ($E_{1/2}$) of **6**−**9** are negatively shifted due to the weaker electron-

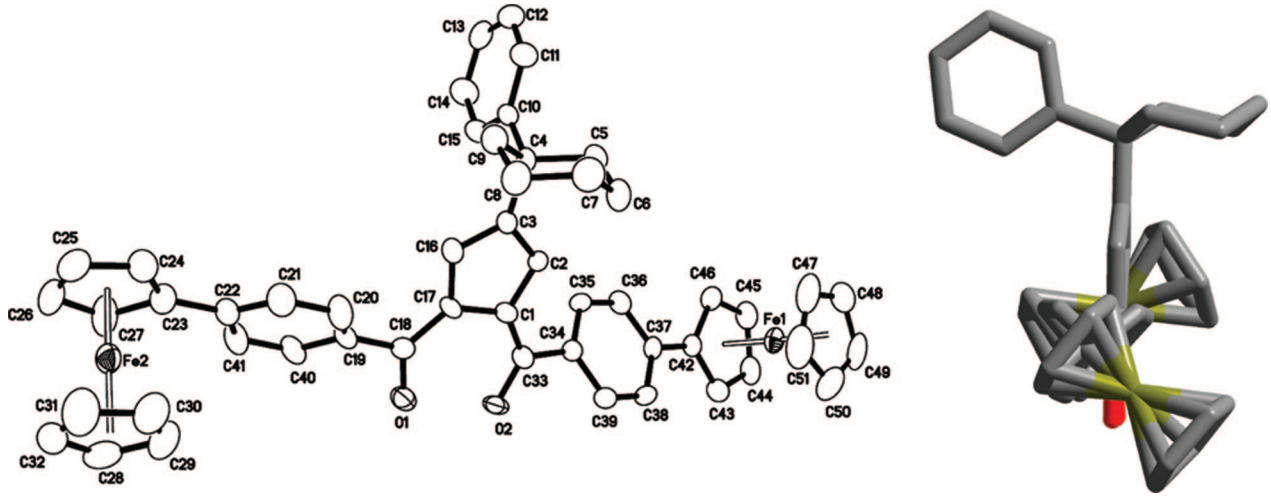

Figure 5. ORTEP drawing and stick representation of **5**.

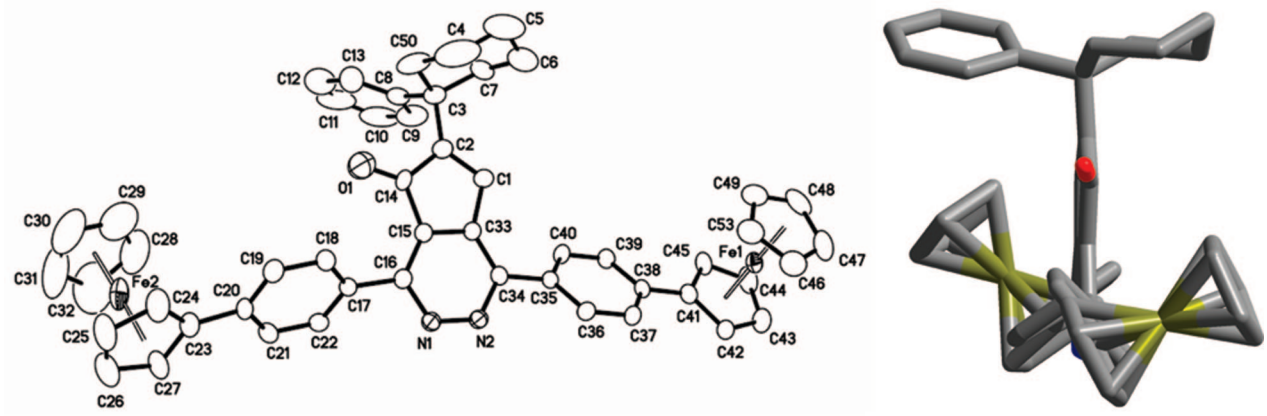

Figure 6. ORTEP drawing and stick representation of **7**.

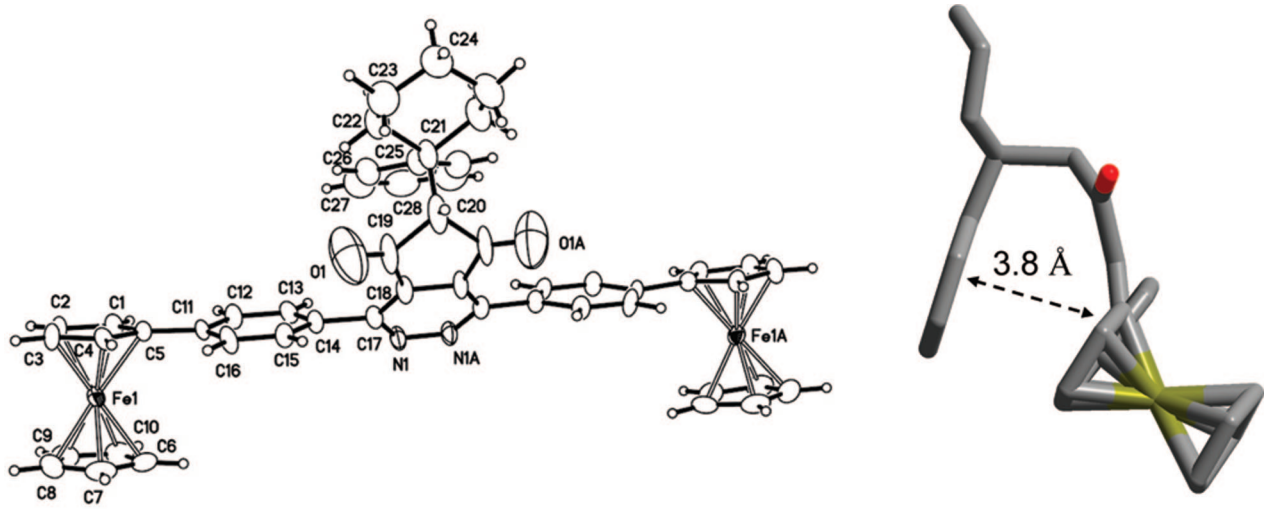

Figure 7. ORTEP drawing and stick representation of **8**.

withdrawing effect of imine caused by the inserted phenyl group. Different from **6**−**8**, compound **9** shows two quasi-reversible redox waves. The $E_{1/2}$ value of 0.707 V is assigned to the Fc attached to the >C═O, which is a strong electron-withdrawing group. The other wave is assigned to the two terminal ferrocenyls attached to the phenyl groups. The inserted phenyl groups significantly reduce the electron-withdrawing effect of the central cyclopenta[*d*]pyridazine moiety, which results in the two terminal ferrocenyl groups being in basically the same electrochemical environment and in a lower *E* value.

Preliminary Theoretical Calculations. To gain a deeper insight into the novel oxidation and hydrolysis reactions, for this study, DFT calculations with the B3LYP functional and the 6-31G(d) basis set were used.[9] Full geometry optimizations without any symmetry constraints were carried out. The calculations were performed with the Gaussian 98 software on

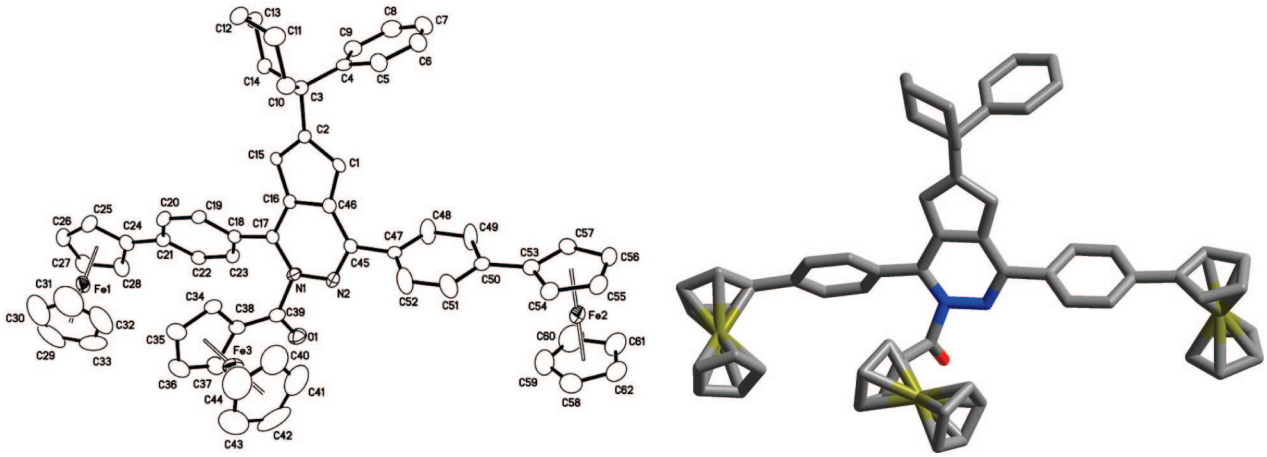

Figure 8. ORTEP drawing and stick representation of **9**.

Table 1. Crystallographic Data for 3−5 and 7−9

empirical formula	$C_{39}H_{34}Fe_2N_2O$	$C_{39}H_{34}Fe_2N_2O_2$	$C_{51}H_{44}Fe_2O_2$	$C_{52}H_{44}Cl_2Fe_2N_2O$	$C_{53}H_{46}Cl_4Fe_2N_2O_2$	$C_{63}H_{54}Cl_2Fe_3N_2O$
	3	**4**	**5**	**7**	**8**	**9**
fw	658.38	674.38	800.56	895.49	996.42	1093.53
cryst syst	triclinic	orthorhombic	triclinic	triclinic	orthorhombic	triclinic
a (Å)	11.231(8)	16.871(2)	10.140(2)	10.438(4)	28.871(7)	12.865(2)
b (Å)	12.606(9)	9.3341(12)	15.103(4)	14.746(5)	7.5729(17)	14.584(3)
c (Å)	12.790(9)	37.956(5)	15.293(4)	14.994(5)	10.514(2)	14.693(3)
α (deg)	114.550(12)	90	117.633(4)	83.396(5)	90	78.951(3)
β (deg)	97.629(12)	90	91.536(5)	71.005(5)	90	72.719(3)
γ (deg)	108.532(12)	90	108.432(4)	73.007(5)	90	87.210(3)
V (Å^3)	1486.3(17)	5977.3(13)	1926.1(8)	2086.4(13)	2298.6(9)	2583.2(8)
space group	$P\bar{1}$	*Pbca*	$P\bar{1}$	$P\bar{1}$	*Pmn*2(1)	*Pmn*2(1)
Z value	2	8	2	2	2	2
ρ calc (g/cm^3)	1.471	1.499	1.380	1.425	1.440	1.406
μ(Mo Kα) (mm^{-1})	1.012	1.011	0.795	0.866	0.908	0.980
temp (K)	293(2)	293(2)	293(2)	293(2)	293(2)	293(2)
no. of observations ($I > 3\sigma$)	5053	5265	6640	7184	4130	9063
final *R* indices [$I > 2\sigma(I)$]:[a] *R*; R_w	0.0833; 0.1408	0.0575; 0.1361	0.0691; 0.1116	0.0823; 0.2308	0.0886; 0.2112	0.0935; 0.2302

[a] $R1 = \sum||F_o| - |F_c||/\sum|F_o|$. $wR2 = \{\sum[w(F_o^2 - F_c^2)^2]/\sum[w(F_o^2)^2]\}^{1/2}$.

a Pentium computer. The calculated results are summarized in Table 3. The highest occupied molecular orbital (HOMO) and lowest unoccupied molecular orbital (LUMO) for **2** and **3** are shown in Figure 9. It was found that the energy of the HOMO of **3** ($E = 2.53$ eV) is lower than that of **2** ($E = 2.66$ eV); moreover, the electron density on the atom B of **3** is low, which indicates this carbon atom is not easy to oxidize. On the other hand, the energy of the LUMO ($E = 4.12$ eV) of **3** is much lower than that of **2** ($E = 6.12$ eV), which means that compound **3** prefers to accept electrons for nucleophilic reactions to take place, such as hydrolyzing reactions. As expected, similar calculated results on compounds **6** and **7** were obtained. Compared to **2**, the energy of the HOMO of **6** is clearly decreased, which means **6** is more difficult to oxidize than **2** due to its large conjugated system. Thus, the theoretical calculations herein provide a supportive trend for the current results and discussion.

Conclusion

In conclusion, a series of Fc-containing cyclopentenone (**3** and **7**) and cyclopentenedione (**4** and **8**) derivatives were synthesized successively from the Fc-containing fulvene molecule based on a very simple approach. The current results demonstrated that ferrocenyl groups play a central role in the formation of the cyclopentenone and cyclopentenedione derivatives. Their structures were further confirmed by X-ray single crystal analysis. The oxidation and hydrolysis reactions based on **2**, **3**, **6**, and **7** are in good agreement with the theoretical calculation. We are currently extending this result by preparing new symmetric and unsymmetric ferrocenyl-containing cyclopentenone and cyclopentenedione derivatives of this type, which are potentially used as electronic microsensors for biological and chemical processes.

Experimental Section

Materials and Methods. Compound **1** was prepared according to literature methods.[6] The inorganic metal salts and organic regents were purchased from Acros and used without further purification. Infrared (IR) samples were prepared as KBr pellets, and spectra were obtained in the 400−4000 cm^{-1} range using a Perkin-Elmer 1600 FTIR spectrometer. ^{1}H NMR data were collected using a JEOL FX 90Q NMR or AM-300 spectrometer. Chemical shifts are reported in δ relative to TMS. Element analyses were performed on a Perkin-Elmer model 240C analyzer. All fluorescence measurements were carried out on a Cary Eclipse spectrofluorimeter (Varian, Australia) equipped with a xenon lamp and quartz carrier at room temperature.

Synthesis of 1. Compound **1** was prepared according to the literature method.[6h] The characterization data of ^{1}H NMR,

(8) (a) Caballero, A.; Lloveras, V.; Tárraga, A.; Espinosa, A.; Velasco, M. D.; Vidal-Gancedo, J.; Rovira, C.; Wurst, K.; Molina, P.; Veciana, J. *Angew. Chem., Int. Ed.* **2005**, *44*, 1977. (b) Martínez, R.; Ratera, I.; Tárraga, A.; Molina, P.; Veciana, J. *Chem. Commun.* **2006**, 3809.

(9) (a) Hohenberg, P.; Kohn, W. *Phys. Rev. B* **1964**, *136*, 864. (b) Kohn, W.; Sham, L. *J. Phys. Rev. A* **1965**, *140*, 1133. (c) Becke, A. D. *J. Chem. Phys.* **1992**, *97*, 9173. (d) Lee, C.; Yang, W.; Parr, R. G. *Phys. Rev. B* **1988**, *37*, 785.

Table 2. Interatomic Distances (Å) and Bond Angles (deg) with esd's for 3−5 and 7−9

		3	
C(1)−O(1)	1.237(8)	C(1)−C(2)	1.505(10)
C(17)−N(1)	1.346(8)	N(1)−N(2)	1.332(8)
Fe(1)−C(31)	2.014(9)	Fe(2)−C(19)	2.046(8)
C(15)−C(2)−C(1)	105.7(7)	O(1)−C(1)−C(2)	125.3(7)
N(1)−C(17)−C(16)	118.5(7)	N(1)−N(2)−C(29)	120.0(6)
		4	
C(3)−O(2)	1.168(6)	C(17)−O(1)	1.212(7)
C(1)−N(1)	1.349(5)	N(1)−N(2)	1.337(4)
Fe(1)−C(26)	2.026(5)	Fe(2)−C(30)	2.025(4)
O(2)−C(3)−C(2)	127.4(4)	O(2)−C(3)−C(4)	123.8(5)
N(2)−N(1)−C(1)	121.0(3)	N(1)−N(2)−C(19)	121.8(3)
		5	
C(18)−O(1)	1.299(6)	C(33)−O(2)	1.279(6)
C(16)−C(17)	1.407(7)	C(22)−C(23)	1.474(8)
Fe(1)−C(50)	2.018(7)	Fe(2)−C(23)	2.022(6)
O(2)−C(33)−C(1)	122.5(5)	O(2)−C(33)−C(34)	115.0(5)
C(2)−C(1)−C(33)	126.0(5)	C(24)−C(23)−C(22)	129.1(7)
		7	
C(14)−O(1)	1.203(7)	N(1)−N(2)	1.329(5)
N(1)−C(16)	1.343(6)	Fe(1)−C(46)	2.012(6)
N(2)−C(34)	1.341(6)	Fe(2)−C(28)	2.022(11)
N(2)−N(1)−C(16)	120.4(4)	N(1)−N(2)−C(34)	121.8(4)
O(1)−C(14)−C(2)	124.5(5)	C(19)−C(20)−C(23)	121.3(5)
		8	
C(19)−O(1)	1.153(14)	N(1)−N(1)#1	1.335(11)
C(17)−N(1)	1.345(10)	Fe(1)−C(3)	2.011(9)
N(1)#1-N(1)−C(17)	121.2(4)	O(1)−C(19)−C(18)	127.7(11)
O(1)−C(19)−C(18)	127.7(11)	C(3)−Fe(1)−C(9)	125.3(4)
		9	
N(1)−N(2)	1.362(7)	C(45)−N(2)	1.325(8)
C(45)−N(2)	1.325(8)	C(34)−Fe(3)	2.014(7)
C(54)−Fe(2)	2.021(8)	C(39)−O(1)	1.210(8)
N(2)−N(1)−C(17)	126.6(5)	N(2)−N(1)−C(39)	109.4(5)
O(1)−C(39)−C(38)	125.0(6)	O(1)−C(39)−N(1)	118.6(6)

Table 3. UV/Vis Absorption Data for Compounds 5−9 in CH_2Cl_2[a]

compound	absorption maxima λ_{max}, nm (ϵ, 10^4 M^{-1} cm^{-1})
5	229 (8.47), 305 (7.07), 451 (5.36)
6	227 (5.09), 308 (6.20), 446 (0.50)
7	229 (6.47), 312 (5.47), 376 (1.97)
8	228 (3.83), 295 (2.59), 342 (2.45), 469 (0.59)
9	228 (5.42), 295 (5.02), 441 (0.59)

[a] From OTTLE spectroelectrochemistry in CH_2Cl_2/0.1 M n-Bu_4NPF_6.

Table 4. Cyclic Voltammogram Data of 6−9

compound	$E_{p,a}$	$E_{p,c}$	$E_{1/2}$ (V)[a]	ΔE_p (mV)[b]	I_{pa}/I_{pc}
6	0.524	0.438	0.481	86	1.09
7	0.524	0.456	0.490	68	0.97
8	0.496	0.430	0.463	66	0.97
9	0.742	0.672	0.707	70	0.94
	0.546	0.454	0.500	92	0.86

[a] $E_{1/2} = E_{p,a} + E_{p,c}/2$. [b] $\Delta E_p = E_{p,a} - E_{p,c}$.

IR, and elemental analysis are consistent with the our previous report.[6h]

Synthesis of 2. A solution of **1** (0.32 g, 0.49 mmol) in anhydrous EtOH (20 mL) and a large excess $N_2H_4 \cdot H_2O$ was heated to reflux for about 24 h. After cooling to room temperature, the solvent was removed under reduced pressure to give a yellow-orange solid. The product was recrystallized from EtOH to give orange crystals of **2** (yield 96%). Mp = 253 °C (dec). IR (KBr pellet cm^{-1}): 3379(vs), 3090(w), 2933(vs), 2855(m), 1594(s), 1517(s), 1492(m), 1454(s), 1369(m), 1335(m), 1166(w), 1104(w), 1030(m), 1002(w), 877(w), 832(m), 752(w), 701(m), 669(w), 637(w), 501(vs). ^{1}H NMR (300 MHz, $CDCl_3$, 25 °C, TMS, ppm): 10.32 (s, 1H, −OH), 7.44−7.11 (m, 5H, $-C_6H_5$), 6.95 (s, 2H, $-C_5H_2$), 4.93−4.12 (s, s, s, 18H, −Fc), 2.46−1.68 (m, 10H, $-C_6H_{10}$). Anal. (%) Calcd for $C_{39}H_{36}N_2Fe_2$: C 72.67, H 5.59, N 4.35. Found: C 72.86, H 5.60, N 4.24.

Synthesis of 3. A solution of **2** in CH_2Cl_2 was stirred at room temperature for 24 h in air, and then the solvent was removed under reduced pressure to give deep green solids. The product was purified by column chromatography on Al_2O_3 (CH_2Cl_2) to afford deep green crystalline solids. Yield: 88%. Mp = 248−250 °C. IR (KBr pellet cm^{-1}): 3092(w), 2929(s), 2855(w), 1713(vs), 1640(m), 1555(vs), 1492(w), 1465(m), 1385(m), 1314(w), 1269(w), 1236(w), 1192(w), 1105(w), 1029(m), 1002(m), 966(w), 909(w), 874(w), 819(s), 729(s), 699(m), 648(w), 561(w), 438(s). ^{1}H NMR (300 MHz, $CDCl_3$, 25 °C, TMS, ppm): 7.69 (s, 1H, $-C_5H$), 7.48−7.22 (m, 5H, $-C_6H_5$), 5.55−4.03 (s, s, d, d, 18H, −Fc), 2.51−1.63 (m, 10H, $-C_6H_{10}$). Anal. (%) Calcd for $C_{39}H_{34}N_2OFe_2$: C 71.12, H 5.17, N 4.26. Found: C 71.34, H 5.26, N 4.15.

Synthesis of 4. A catalytic amount of $SnCl_2$ and several drops of water were added to a solution of **3** (0.18 g, 0.27 mmol) in anhydrous EtOH (100 mL), and the mixture was stirred at room temperature for 12 h. Solvent was removed under reduced pressure to give purple crystalline solids. The product was purified by column chromatography on Al_2O_3 (CH_2Cl_2) to afford purple crystalline solids. Yield: 75%. Mp = 234−236 °C. IR (KBr pellet cm^{-1}): 3090(w), 2925(vs), 2854(s), 1715(vs), 1635(m), 1537(s), 1495(w), 1467(s), 1385(s), 1341(m), 1318(w), 1249(w), 1197(w), 1160(w), 1127(w), 1104(m), 1056(w), 1026(m), 1002(m), 879(w), 866(w), 818(s), 761(w), 735(w), 704(s), 615(w), 555(w), 524(w), 502(s), 482(s). ^{1}H NMR (300 MHz, $CDCl_3$, 25 °C, TMS, ppm): 7.42−7.10 (m, 5H, $-C_6H_5$), 5.58−4.00 (s, s, s, d, d, 18H, −Fc), 3.17−1.44 (m, 10H, $-C_6H_{10}$). Anal. (%) Calcd for $C_{39}H_{33}N_2O_2Fe_2$: C 69.54, H 4.90, N 4.16. Found: C 69.65, H 4.78, N 4.24.

Synthesis of 5. The process was the same as that for **1** but used FcC_6H_4COCl rather than FcCOCl as the starting material. Yield: 25.0%. Mp = 198 °C (dec). IR (KBr pellet cm^{-1}): 2928(m), 2854(w), 1625(s), 1603(vs), 1494(m), 1406(s), 1346(s), 1267(m), 1175(m), 1106(w), 882(w), 828(m), 670(s), 484(m). ^{1}H NMR (300 MHz, $CDCl_3$, 25 °C, TMS, ppm): 18.26 (s, 1H, −OH), 7.71−7.52 (m, 8H, $-C_6H_4$), 7.28−7.12 (m, 5H, $-C_6H_5$), 7.12 (s, 2H, $-C_5H_2$), 4.77−4.12 (m, 18H, −Cp), 2.17−1.57 (m, 10H, $-C_6H_{10}$). Anal. (%) Calcd for $C_{51}H_{44}O_2Fe_2$: C 76.50, H 5.50. Found: C 76.56, H 5.28.

Synthesis of 6. The process was the same as that for **2** but used **5** rather than **1** as the starting material. Yield: 92.3%. Mp = 270 °C (dec). IR (KBr pellet cm^{-1}): 3414(s), 3091(s), 2930(vs), 2855(m), 1607(s), 1515(s), 1450(vs), 1369(vs), 1282(m), 1186(w), 1109(m), 1077(m), 1003(m), 947(w), 887(w), 833(s), 752(w), 698(s), 673(m), 534(w), 507(m), 462(w). ^{1}H NMR (300 MHz, $CDCl_3$, 25 °C, TMS, ppm): 10.63 (s, 1H, −NH), 7.84−7.62 (m, 8H, $-C_6H_4$), 7.39−7.07 (m, 5H, $-C_6H_5$), 6.97 (s, 2H, $-C_5H_2$), 4.76−4.10 (m, 18H, −Cp), 2.50−1.64 (m, 10H, $-C_6H_{10}$). Anal. (%) Calcd for $C_{51}H_{44}N_2Fe_2$: C 76.88, H 5.53, N 3.52. Found: C 76.78, H 5.40, N 3.38.

Synthesis of 7. The process was the same as that for **3** but used **6** rather than **2** as the starting material. In addition, the reaction time is 72 h instead of 24 h. Yield: 64.6%. Mp = 260 °C (dec). IR (KBr pellet cm^{-1}) 3090(w), 2928(s), 2855(m), 1719(vs), 1608(vs), 1572(w), 1520(m), 1494(w), 1445(w), 1414(w), 1358(s), 1280(w), 1230(w), 1187(w), 1106(m), 1032(m), 1015(m), 886(m), 820(s), 757(w), 698(m), 665(w), 488(m). ^{1}H NMR (300 MHz, $CDCl_3$, 25 °C, TMS, ppm): 7.94−7.54 (m, 8H, $-C_6H_4$), 7.63 (s, 1H, $-C_5H$), 7.42−7.17 (m, 5H, $-C_6H_5$), 4.79−4.13 (m, 18H, −Cp), 2.37−1.59 (m, 10H, $-C_6H_{10}$). Anal. (%) Calcd for $C_{51}H_{42}N_2OFe_2$: C 75.56, H 5.18, N 3.46. Found: C 75.48, H 5.07, N 3.35.

Synthesis of 8. The process was the same as that for **4** but used **7** rather than **3** as the starting material. Yield: 50.2%. Mp = 220 °C (dec). IR (KBr pellet cm^{-1}): 3090(w), 2930(m), 2857(w), 1721(vs), 1607(vs), 1517(w), 1452(w), 1417(m), 1383(vs), 1281(w),

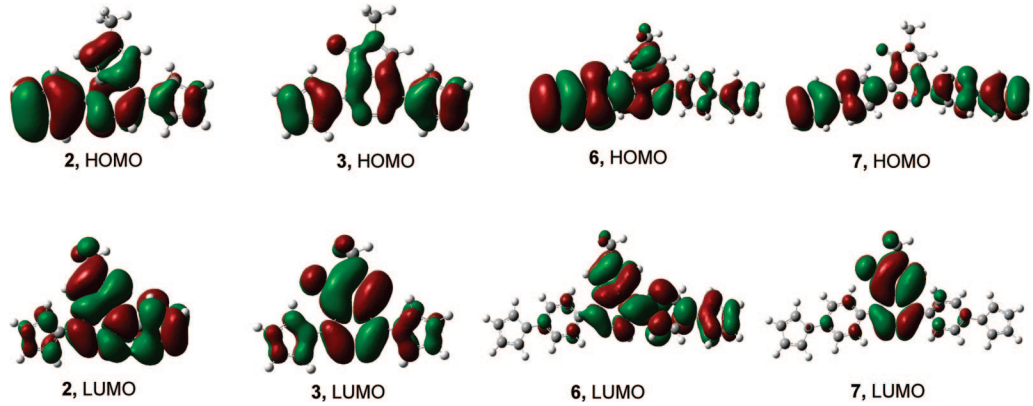

Figure 9. HOMO and LUMO of **2**, **3**, **6**, and **7**.

Table 5. Calculation Results for 2, 3, 6, and 7[a]

	2	3	6	7
HOMO (*E*/eV)	2.66	2.53	1.22	1.00
LUMO (*E*/eV)	6.12	4.12	3.53	2.00
charge of atom A	−0.316	0.303	−0.306	0.322
charge of atom B	−0.314	−0.143	−0.304	−0.138

[a] Charge = −2; singlet. Atoms A and B are marked in Schemes1 and 2.

1188(m), 1137(w), 1103(s), 1083(m), 1030(m), 1015(m), 886(m), 840(s), 827(s), 765(w), 732(vs), 704(s), 645(w), 515(s), 482(m), 453(w). ^{1}H NMR (300 MHz, $CDCl_3$, 25 °C, TMS, ppm): 7.81−7.61 (m, 8H, $-C_6H_4$), 7.28−7.00 (m, 5H, $-C_6H_5$), 4.74−4.08 (m, 18H, −Cp), 3.15−1.38 (m, 10H, $-C_6H_{10}$). Anal. (%) Calcd for $C_{51}H_{41}N_2O_2Fe_2$: C 74.18, H 4.97, N 3.39. Found: C 74.09, H 4.58, N 3.41.

Synthesis of 9. FcC_6H_4COCl (0.14 g, 0.57 mmol) was added to a solution of **6** (0.15 g, 0.19 mmol) in CH_2Cl_2 (30 mL). The mixture was stirred for 24 h at room temperature. Solvent was removed under vacuum to give orange crystalline solids. The product was purified by column chromatography on silica gel (CH_2Cl_2) to afford yellow-orange crystalline solids. Yield: 54.7%. IR (KBr pellet cm^{-1}): 2927(s), 2854(m), 1710(s), 1607(s), 1522(m), 1443(s), 1401(vs), 1321(s), 1258(vs), 1185(w), 1082(s), 1054(m), 1028(m), 1001(s), 868(m), 820(s), 754(s), 733(m), 699(m), 489(s). ^{1}H NMR (300 MHz, $CDCl_3$, 25 °C, TMS, ppm): 7.97−7.08 (m, 13H, $-C_6H_4$, $-C_6H_5$), 6.95, 6.69 (s, s, 2H, $-C_5H_2$), 4.81−4.02 (m, 27H, −Cp), 2.38−1.61 (m, 10H, $-C_6H_{10}$). Anal. (%) Calcd for $C_{62}H_{52}N_2OFe_3$: C 73.81, H 5.16. Found: C 73.72, H 5.14.

Single-Crystal Structure Determination. Single crystals of **3**−**5** and **7**−**9** were obtained by the slow evaporation of a CH_2Cl_2/EtOH solution. Suitable single crystals of **3**−**5** and **7**−**9** were selected and mounted in air onto thin glass fibers. X-ray intensity data were measured at 293(2) K on a Bruker SMART APEX CCD-based diffractometer (Mo Kα radiation, $\lambda = 0.71073$ Å). The raw frame data for **3** and **4** were integrated into SHELX-format reflection files and corrected for Lorentz and polarization effects using SAINT.[10] Corrections for incident and diffracted beam absorption effects were applied using SADABS.[10] None of the crystals showed evidence of crystal decay during data collection. The structure was solved by a combination of direct methods and difference Fourier syntheses and refined against F^2 by the full-matrix least-squares technique. Crystal data, data collection parameters, and refinement statistics for **3**−**5** and **7**−**9** are listed in Tables 1 and 2.

Acknowledgment. We are grateful for financial support from the National Natural Science Foundation of China (Grant Nos. 20871076 and 20671060), National Basic Research Program of China (973 Program, 2007CB936000), and Shangdong Natural Science Foundation (Nos. J06D05, 2006BS04040, and 2007BS04002).

Supporting Information Available: Crystallographic information files (CIF). This material is available free of charge via the Internet at http://pubs.acs.org.

OM800246S

(10) *SAINT*; Bruker Analytical X-ray Systems, Inc.: Madison, WI, 1998.